Received: 9 July 2021 | Revised: 11 November 2021 | Accepted: 10 January 2022

DOI: 10.1002/we.2712

RESEARCH ARTICLE

WILEY

Sensitivity of the dynamic response of a multimegawatt floating wind turbine to the choice of turbulence model

Astrid Nybø[1] | Finn Gunnar Nielsen[1] | Marte Godvik[1,2]

[1]Geophysical Institute and Bergen Offshore Wind Centre (BOW), University of Bergen, Bergen, Norway

[2]Equinor, Stavanger, Norway

Correspondence
Astrid Nybø, Geophysical Institute and Bergen Offshore Wind Centre (BOW), University of Bergen, Allégaten 70, Bergen 5007, Norway.
Email: astrid.nybo@uib.no

Abstract

In the design of offshore wind turbines, it is important to make a realistic estimate of the wind load. This is particularly important for floating wind turbines, having natural frequencies in a frequency range where the wind loads are high and large turbulent structures exist. This study shows that turbulence modelling greatly impacts the response of a 15-MW floating wind turbine. The turbulence models recommended by the International Electrotechnical Commission (IEC) are challenged by considering two additional models: Large Eddy Simulations (LES) and an approach using input from offshore wind measurements (TIMESR). The two standard models, the Kaimal spectrum with IEC coherence model (Kaimal) and the Mann spectral tensor model (Mann), differ in their coherence formulation. This results in higher standard deviations for the surge and pitch motions, and lower for the yaw motion, when applying Kaimal in comparison to Mann. For the specific floater of this study, more damage is obtained in the mooring lines when applying Kaimal. Applying the more realistic models, LES and TIMESR, increases the range of response further, concluding that the two standard turbulence models may lead to incorrect estimations of the response of a floating wind turbine. LES and TIMESR take atmospheric stability into account, which is proven to alter the response significantly.

KEYWORDS
coherence, floating wind turbines, spectral response, turbulence models

1 | INTRODUCTION

Several recent reports[1–3] point towards energy from offshore wind as a key resource in the future renewable energy market. The cost of energy from offshore wind has been reduced significantly over the last years, and this trend is expected to continue. A key to this cost reduction is the development of larger wind turbines with corresponding large rotors. Rotor diameters in excess of 200 m are now state of art. The availability of shallow water areas with good wind conditions is limited; however, worldwide huge deep-water areas suited for floating wind turbines are available. Thus, the understanding of the dynamic behaviour of wind turbines on floating support structures is important.

For large rotors, a good understanding of the wind induced loads is important to obtain proper estimates of the dynamics of the support structure and the corresponding fatigue damage. The wind industry relies upon standards from, for example, the International Electrotechnical Commission[4–6] (IEC) for wind turbine design. These standards recommend two simplistic turbulence models for estimating wind loads over periods between minutes and hours. These models are the Kaimal wind spectrum[7] combined with an exponential coherence model, in the

following referred to as 'Kaimal', and the Mann spectral tensor model,[8] in the following referred to as 'Mann'. More complex models like Large Eddy Simulations (LES) are able to create wind fields in a more realistic manner. Their large disadvantage, however, is the additional computational effort required. An additional option is to use wind time series and coherence as obtained from measurements. Here, the challenge is to construct a complete wind field from a few point measurements. A procedure for this is implemented in the method referred to as 'TIMESR' by TurbSim.[9]

A previous study by Nybø et al.[10] shows that the turbulent characteristics of the Kaimal, Mann, LES and TIMESR wind fields vary significantly. The coherent structures over the rotor plane are modelled differently. In contrast to Kaimal and Mann, TIMESR and LES can take atmospheric stability into account when modelling the eddies of the wind fields. In TIMESR, coherence estimates obtained from measured time series in various atmospheric stability conditions may be fitted to a coherence model and used in the generation of eddies. A stable atmosphere is typically characterised by low turbulence levels, high variation of wind speed with height and small eddies. An unstable atmosphere, on the other hand, has higher turbulence levels, lower variation of wind speed with height and large long-lasting coherent structures. In the North Sea, stable conditions are typically obtained in summer, when warm air is transported over cold sea. Similarly, unstable conditions are typically obtained during winter when cold wind blows over warm sea.

The differences in wind characteristics across turbulence models impact the dynamic response of offshore wind turbines. The variation of wind speed over the rotor is greater for larger wind turbines, typically placed offshore, than for small onshore wind turbines developed decades ago. With larger offshore wind turbines, it becomes more important to model these wind variations correctly. Nybø et al.,[11] evaluated the differences in response of a large bottom-fixed wind turbine using Kaimal, Mann, LES and TIMESR wind fields. Significant differences were found in the response, even in wind fields with similar wind speeds and turbulence levels at hub height. It was found that differences in coherent structures have large impact on differences in response for all atmospheric stability conditions. Coherent wind fields cause, for example, larger tower bottom fore-aft bending moments, while less coherent wind fields cause larger tower yaw bending moments.

Nybø et al.[11] found that the differences in response of using the different turbulence models are mainly seen at frequencies below 0.1 Hz. Most of the energy in the wind spectra and most of the large coherent structures are present in this frequency region. In contrast to bottom-fixed wind turbines, studied by Nybø et al.,[11] floating wind turbines have natural frequencies at low frequencies. The natural frequencies of the floater motions surge, pitch and heave have major impact on the response of a floater. As these natural frequencies are found in the low-frequency region where the wind load is high and the modelling of coherent structures varies significantly across turbulence models, even larger differences in response are expected when using different wind fields for floating wind turbines. The impact of turbulence models on the dynamic response of floating wind turbines is documented by previous studies.[12–18]

In the present study, the differences in response of using Kaimal, Mann, TIMESR and LES are evaluated in terms of standard deviation (STD) of the motions of the support structure. Further, the damage equivalent load (DEL) in the upper part of the most heavily loaded mooring line is computed. The differences in STD of motions and DEL obtained using the various wind fields are evaluated in various wind speeds and atmospheric stability conditions. In order to properly understand the origin of the differences, the impact of wind shear, turbulence level and especially coherence on response is tested for the specific structure.

In comparison to the previous studies mentioned above, a larger wind turbine is analysed in the present study. The IEA 15-MW[19] has a rotor size which is expected to be relevant for commercial scale in a few years. This turbine together with the Windcrete[20] spar foundation is analysed in the present study. Using both turbulence models recommended by the standard, an LES model and a model based on measurements for floater response comparisons, also makes this study unique in comparison to the previous studies mentioned above. Last, the present study uniquely supports its conclusions by a thorough analysis of the impact of specific wind characteristics on floating wind turbine response.

2 | DATA AND METHODS

In the following, the wind fields used in this study, TIMESR, Kaimal, Mann and LES, are introduced. Basic equations and principles are given in order to compare these wind fields in various stability and wind speed situations. The differences in wind fields are analysed by the turbulence intensity and wind spectrum at hub and coherence over a distance in the order of the rotor diameter.

Furthermore, the offshore wind turbine in consideration is introduced together with the simulation software and corresponding simulation choices. The response parameters and statistical parameters of the response analysis are defined.

2.1 | Wind fields

The TIMESR, Kaimal, Mann and LES wind fields are all simulated for situations covering three wind speeds and three stability conditions. The main wind characteristics of these situations and other main specifics of the domain are covered in Table 1. The three wind speed situations are run in neutral conditions, which Kaimal and Mann are originally intended for. The three situations of different atmospheric stability are run at just above rated wind speed where the wind turbine experiences high loads.

TABLE 1 Summary of wind field characteristics

	7 m/s	13 m/s			18 m/s
	Neutral	Stable	Neutral	Unstable	Neutral
Mean wind speed at 135 m	7.4–7.5 m/s	12.9–13.0 m/s	12.5 m/s	12.6 m/s	17.7–18.1 m/s
Turbulence intensity at 135 m	3.6–5.7%	2.0–2.8%	3.0–5.9%	5.5–6.1%	4.6–6.6 %
Power law exponent	0.04	0.2	0.05–0.06	0.02–0.03	0.06
Obukhov length (TIMESR & LES)	−1107 & −798	158 & 86	2753 & −1049	−451 & −56	2051 & −1208
			All		
Grid size horizontally and vertically			4.2 m		
Domain size horizontally and vertically			264.6 m		
Simulation time			1 h		
Time step			0.1 s		

Note: The ranges given for mean wind speed and TI are the ranges obtained in analysing the generated wind fields. The stable and unstable Mann and Kaimal wind fields should be considered as neutral flows with TI and wind profiles adapted to the given stability, and thus, the Obukhov lengths are not given for these wind fields. The resolution and domain of LES are originally larger than indicated in this table, but interpolations are performed in order to compare at the same grounds.

The mean wind speed in the mean wind direction, $\overline{u}$, together with the STD, σ_u, defines the turbulence intensity, *TI*, by

$$TI = \frac{\sigma_u}{\overline{u}}. \tag{1}$$

$\overline{u}$ and TI are referred to hub height in the following. TI is calculated from 1-Hz data averaged over 10 min. The wind profile is defined by the power law exponent, α, in Table 1, which is given by Equation (2).

$$\overline{u}(z) = \overline{u}_{ref}\left(\frac{z}{z_{ref}}\right)^{\alpha}. \tag{2}$$

$\overline{u}$ is the mean wind speed at height z, and $\overline{u}_{ref}$ is the wind speed at a reference height, z_{ref}. The power law exponents are calculated from mean wind speeds at 40 and 80 m. The atmospheric stability condition is given by the Obukhov length,[21] *L*, in Table 1. It relates buoyancy and shear effects in the generation of turbulence, and is given by Equation (3).

$$L = \frac{-\overline{\theta_v}u_*^3}{kg\left(\overline{w'\theta'}\right)_s}. \tag{3}$$

$\overline{\theta_v}$ is the virtual potential temperature, u_* is the friction velocity defined by Equation (4), k is the von Karman constant, g is the gravitational constant, $\left(\overline{w'\theta'}\right)_s$ is the surface vertical kinematic eddy heat flux and u', v' and w' are the longitudinal, lateral and vertical velocity fluctuations, respectively.

$$u_*^2 = \sqrt{\overline{u'w'}^2 + \overline{v'w'}^2}. \tag{4}$$

The Obukhov length is calculated with a reference height 40 m above sea level. In accordance with van Wijk et al.,[22] the atmosphere is considered near-neutral when the absolute value of the Obukhov length is above 1000, that is, low effect of buoyancy. A negative value closer to zero corresponds to an unstable atmosphere, while a positive value closer to zero corresponds to a stable atmosphere. The LES wind field at 7 m/s is not neutral according to these limits. The Obukhov length is rather low as a positive surface heat flux had to be added in order to achieve an acceptable turbulence intensity. This case is still considered neutral in the current study, as the absolute value of the Obukhov length is far from zero.

The TIMESR and Kaimal wind fields are generated by Turbsim,[9] Mann by the DTU Mann generator[23] and LES by SOWFA.[24] A short description of the generation of the different wind fields is summarized under 'Response analysis' in Table 2. The coherence, which is referred to

TABLE 2 Summary of simulated wind fields

Method	Description	Seeds
Response analysis		
TIMESR	Wind spectra interpolated in space and Davenport coherence model	6/case
Kaimal	Kaimal wind spectrum and IEC exponential coherence model	6/case
Mann	Mann wind spectrum and coherence model	6/case
LES	Computational fluid dynamics	1/case
Wind characteristics test (just above rated wind speed)		
Uniform	No wind shear or turbulence	1
Wind shear	No turbulence, but wind shear similar to Kaimal[a] neutral wind field	1
Fully coherent	TS from hub height of Kaimal[a] neutral wind field	1
Horizontally coherent	TS from horizontal centre of Kaimal[a] neutral wind field repeated horizontally	1
Vertically coherent	TS from vertical centre of Kaimal[a] neutral wind field repeated vertically (+shear)	1
Negative coherence	Kaimal spectrum with $\mathrm{Re}[\gamma_y]$ from Equation (7), with $C_1 = 4\pi$, $C_2 = 5$ and $C_3 = 0.035$	6
Neg. coh. = 0	Same as 'Negative coherence' but $\mathrm{Re}[\gamma_y] < 0$ replaced by 0	6
Neg. coh = pos. coh.	Same as 'Negative coherence' but $\mathrm{Re}[\gamma_y] < 0$ replaced by positive equivalent	6

[a]Refers to the Kaimal wind spectrum and IEC exponential coherence model.
Note: TS = time series, case = wind speed and stability situation, neg. = negative, pos. = positive, coh. = coherence.

TABLE 3 Inputs to TIMESR, Kaimal, Mann and LES turbulence models

Method	Inputs
TIMESR	Wind speed time series, profile coefficients and Davenport coherence parameters from measurements
Kaimal	Mean wind speed, TI and power law coefficient from TIMESR
Mann	Mean wind speed, TI and power law coefficient from TIMESR
LES	Atmospheric input conditions giving similar stability, wind speed profile and TI to TIMESR

in this table, describes the frequency dependent correlation between two time series separated in space. Spatial coherence in all directions is present in all the wind fields considered. In the results of this study, only the real part of the coherence of the along wind component, the uu-co-coherence, is presented; thus, any reference to coherence corresponds to this parameter. It is given by Equation (5), where S_{ii} and S_{jj} are one-sided auto-spectra of the wind velocities at two different positions, i and j, and S_{ij} is the cross spectrum between these two.

$$\mathrm{Re}(\gamma) = \mathrm{Re}\left(\frac{S_{ij}}{\sqrt{S_{ii}S_{jj}}}\right). \tag{5}$$

Sonic anemometer measurements from the offshore mast FINO1,[25,26] located in the North Sea close to Germany, are used to generate the various wind fields according to Table 3. In TIMESR, the time series from three point measurements separated vertically are used directly. The Davenport coherence model (Equation 6) is used, where C is the decay coefficient obtained from measurements, f is the frequency, δ is the separation distance between the two points considered and $\overline{u}_m$ is the mean wind speed between them.

$$\gamma = \exp\left(-C\frac{f\delta}{\overline{u}_m}\right). \tag{6}$$

The Davenport model is a very simple model for estimating coherence. It is still found to fit well to measurements of the uu-coherence at FINO1 as shown by Cheynet et al.[27] and exemplified by Nybø et al.[10] The TIMESR model is the only model of this study taking measurements into account in the estimation of coherence. The mean wind speeds, TI and power law coefficients, used as inputs in Kaimal and Mann, vary with the different wind speed and stability situations. The Kaimal and Mann wind fields are in this study generated according to the IEC standard[4]; thus, the coherent structures do not depend on atmospheric stability. It is possible to fit input parameters of these models to different

atmospheric stability conditions, but this is not an inherent part of the models. Detailed information about the wind fields may be found in Nybø et al.[10] The wind fields of the present study are generated in a similar manner but for a larger domain customized to a larger wind turbine.

In order to see the isolated effects of wind shear, turbulence and coherence on the response of the 15-MW floating wind turbine, the wind fields under 'Wind characteristics test' of Table 2 are simulated. The impact of coherence is tested in detail, covering the impact of low/high positive coherence, horizontal/vertical separation distance and negative/zero/positive coherence. The wind fields of the two first rows of 'Wind characteristics test' of Table 2 are generated in OpenFAST[28] (see Section 2.2), the wind fields of rows 3–5 from a Kaimal wind field (Kaimal wind spectrum and IEC exponential coherence model) and the wind fields of rows 6–8 from the principles outlined by Cheynet et al.[29]

Cheynet et al. propose the relation given by Equation (7) for the co-coherence, where δ_y is a horizontal separation direction and the Cs are decay coefficients. As observed from the expression, the co-coherence becomes negative at certain frequencies. Using the Cs of Table 2, the negative coherence corresponds well with the results of Mann's formulation. The coherence formulation given by Equation (7) is only used to evaluate the impact of negative coherence in the present study.

$$\mathrm{Re}[\gamma_y] = \cos\left(C_1 \frac{f\delta_y}{\overline{u}}\right) \exp\left(-\frac{\delta_y \sqrt{(C_2 f)^2 + C_3^2}}{\overline{u}}\right). \tag{7}$$

In Nybø et al.,[11] the impact of the imaginary part of the coherence, the quad-coherence, on response was thoroughly investigated. A similar test is performed for the floater of the present study. As in Nybø et al.,[11] negligible effects of quad-coherence are observed; thus, the details of these results are omitted from the following discussion.

It was found in Nybø et al.[11] that six 1-h realizations of the wind fields are needed. The different realizations are obtained by picking random seed numbers in generating random phases for the velocity time series. Still, LES is only run with one seed due to the computational effort required. Some of the wind characteristics test methods are also run with only one seed. This is because their characteristics differ distinctively; thus, statistical certainty is achieved in the corresponding response comparisons even when only one realization is used.

The wind spectra of varying wind speeds and stability conditions are shown in Figure 1. The wind spectra are estimated using Welch's algorithm[30] with a Hamming window, six segments, and 50% overlapping. For all cases, the Kaimal and Mann wind spectra are almost identical to each other. This is according to expectations as the Mann inputs are found by a fit to the Kaimal spectrum according to the IEC-61400.[4] The figure furthermore shows that TIMESR has high energy levels at the very lowest frequencies in most cases. One-hour measured wind time series are used as input to TIMESR. The wind spectra of the measured wind speeds at 40-, 60- and 80-m elevation are reproduced by TIMESR. At the reference height, 80 m, also the time series is reproduced. The measurements may have large scale fluctuations even though the chosen time series are considered stationary based on the criteria given in Nybø et al.[26] These criteria define stationarity based on the linear trends and moving statistics of the time series. The lower limit of frequency considered in the spectral figures is 0.0017 Hz. This corresponds to a block length in the Fast Fourier Transform (FFT) of approximately 10 min. Using a longer block length in the FFT, the extreme values observed at 0.0017 Hz are moved to even lower frequencies, but the same trends are observed. The upper limit is chosen at 0.05 Hz as the highest energy levels are present below this limit. The energy levels increase from low to high wind speeds and stable to unstable situations for all wind fields (note the different scales).

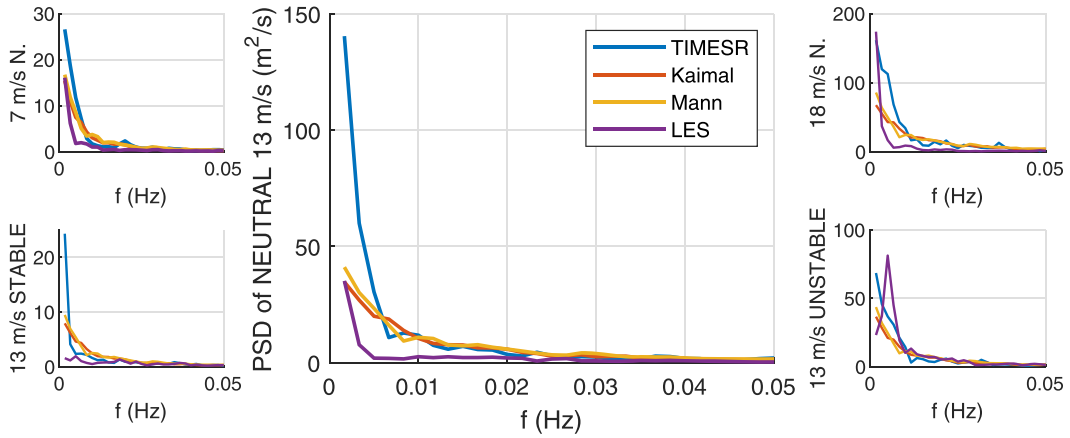

FIGURE 1 Wind spectra at hub height. Top plots, from left to right: 7, 13 and 18 m/s, all neutral stability conditions. Bottom plots, from left to right: stable, neutral and unstable stability conditions, all 13 m/s. PSD = power spectral densities, N. = neutral

Table 1 shows a range of TI for each wind speed and stability situation. All situations have TI that are typical for the given wind speed and stability at FINO1.[10] The chosen unstable situation has a rather low TI in comparison to other unstable situations with a wind speed of about 13 m/s but still typical. Situations with very high TI tend to be non-stationary and are therefore disregarded. The LES wind fields have TI far below the TIMESR, Kaimal and Mann wind fields. It was a challenge to achieve desired TI especially in the neutral situations of LES. The TI is an output rather than input of LES. The obtained TI is sensitive to the surface roughness and surface heat flux. These parameters were tuned to obtain the desired TI and still satisfying the criteria of a neutral stability and desired wind shear. In reality, neutral atmospheric stability conditions rarely exist. It is often a brief period of time as the atmospheric boundary layer (ABL) transitions from one stability to another. The assumptions of a 'canonical' LES applied in this study do not hold in such a transitional state. These assumptions are flow in quasi-equilibrium state, driving pressure gradient constant with height, horizontally homogeneous flow and flow over waves represented by flow over a flat very low roughness wall. As limited information is available from FINO1, the reasons for high TI in neutral conditions are uncertain, and the corresponding atmospheric input conditions to LES are limited. This explains the large differences in TI between LES and the other wind fields in the neutral situations, which are also reflected in the wind spectra.

The coherence of a vertical and horizontal separation distance of 168 m (0.7 rotor diameters) is shown in Figures 2 and 3, respectively. The coherence typically starts off at a high value for low frequencies, decaying towards 0 with increasing frequencies. At frequencies higher than the maximum value in the figures (0.05 Hz), the decay continues. The coherence of distances between the radius and the diameter of the rotor is expected to be highly relevant for response. With smaller separation distances, the curves of Figures 2 and 3 are stretched towards higher frequencies. The same stretching is seen for increasing wind speed, shown by higher coherence at higher frequencies for 18 than 7 m/s. The

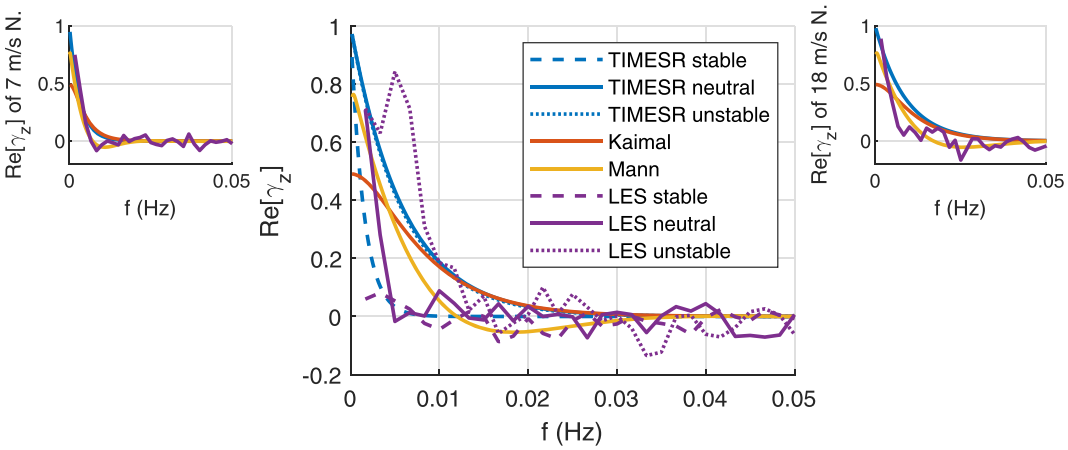

FIGURE 2 Vertical coherence of 0.7 D (168 m). The coherence of the wind fields of various atmospheric stability conditions are all shown in the mid figure. The coherence of Kaimal and Mann is independent of stability. The solid blue line lies on top of the dotted blue line. N. = neutral

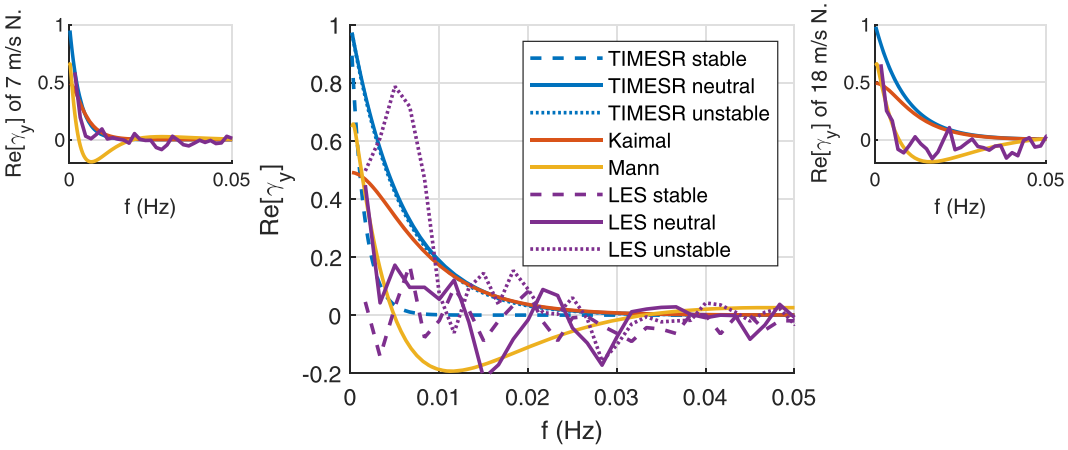

FIGURE 3 Horizontal coherence of 0.7 D (168 m). The coherence of the wind fields of various atmospheric stability conditions are all shown in the mid figure. The coherence of Kaimal and Mann is independent of stability. The solid blue line lies on top of the dotted blue line. N. = neutral

coherence increases from stable to unstable atmospheric conditions. This is especially clear for LES, where the stable situation has close to zero coherence in the whole frequency range. The coherence of the neutral 13 m/s TIMESR wind field is close to the unstable. The stable TIMESR situation has significantly lower coherence than the neutral and unstable situations, but it starts off at unity. This is an assumption and a limitation of the Davenport coherence model used in TIMESR. Kaimal and Mann are independent of atmospheric stability. In contrast to the observations of the wind spectra (Figure 1), significant differences between these two models are observed in the vertical and horizontal coherence (Figures 2 and 3). Mann has a much lower coherence than Kaimal, even negative at some frequencies. This difference is larger with horizontal separation distance. In fact, the coherence of Kaimal and TIMESR are independent on the direction of the separation distance, while significant differences are observed both for Mann and LES. To sum up, the coherence of TIMESR and LES in the stable situation is low. In fact, LES and especially Mann have low coherence in all situations except LES in the unstable situation. The coherence of TIMESR neutral, TIMESR unstable and Kaimal are intermediate and rather similar.

2.2 | Structure and response characteristics considered

The wind turbine structure used in this study corresponds to the IEA 15-MW reference turbine[19] supported by the WindCrete floater,[20] as shown in Figure 4. The rotor diameter is 240 m and the rated wind speed is 10.59 m/s. More information on the rotor specifics is found in Gaertner et al.[19] The WindCrete floater is a 155-m-deep spar structure made from concrete. It has three main mooring lines with delta connections towards the floater. The design is carried out for a Gran Canaria site with a water depth of 200 m. The natural periods with a passive rotor are found to be about 78 s for surge and sway, 42 s for pitch and roll, 34 s for heave and 11 s for yaw. The IEA 15-MW reference tower has been replaced by a concrete tower with a hub height of 135 m in the WindCrete design.

NREL's Reference OpenSource Controller (ROSCO[32]) with variable speed torque control below rated wind speed and collective blade pitch control (constant torque) above rated wind speed is used. The proportional and integral gains of the pitch controller are tuned by the Ziegler–Nichols method[33] for the specific structure in order to avoid instabilities in the platform pitch motion. This is a simplistic approach for handling possible dynamic instabilities of the floater motions. More advanced controller options are discussed in, for example, Skaare et al.[34,35] The signals are filtered prior to input to the controller. The period of the second-order low-pass filter used is 14 s. The controller is thus active at all natural periods important for response but does not react on wave induced motions. Due to the simplistic control system, some unexpected fluctuations in power appear when the wind turbine is subject to turbulent wind. These fluctuations are, however, not considered to influence the computed motion responses to any significant degree. The 13 m/s wind speed case is close to rated wind speed. However, throughout the simulations, a constant torque is observed, proving that the controller is staying in the 'above rated state'. More information on the controller used, hydrodynamics, mooring system and tower are found in Mahfouz et al.[20]

The aero-hydro-servo-elastic tool OpenFAST[28] is used for analysing the response of the wind turbine. The various wind fields are used as inputs to this software. In the LES, the three velocity components are stored at an yz-plane (x = constant) each time step. The stored velocity time series are subsequently transformed to a 'wind-box' on 'Mann-format' to be read by OpenFAST. The aerodynamic loads on the structure are calculated by the blade element momentum theory. The simulations are run for 3800 s. The first 200 s are discarded to remove transient effects. A time step of 0.01 s is used.

In this work, the focus is on floater specific response, more specifically on mooring line tensions and rigid body motions of the floater. Only the dynamic response is analysed in the results section; thus, any reference to response corresponds to dynamic response. Mean motions and mean tensions are only included in response probability distributions. The same trends are seen in the tensions of the six bridle lines and the three

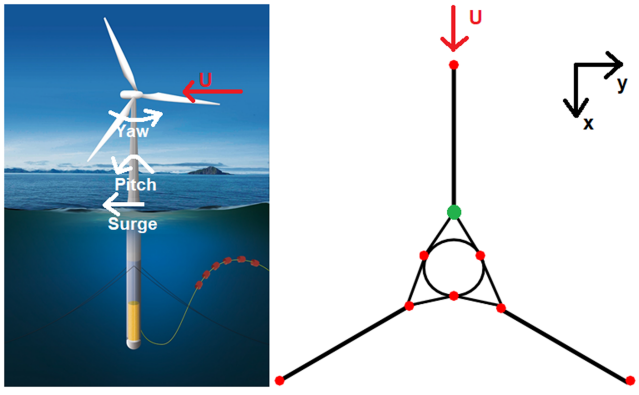

FIGURE 4 Scheme of the Windcrete model, including rigid body motions and mooring layout31

mooring lines. The tension is largest at the connection point between the bridles and the mooring line in front of the wind turbine in the mean wind direction (green dot of Figure 4); thus, this tension is presented in the following. Godvik[16] found strong similarities in bridle tension and yaw motion. In our results, the yaw motion is dominated by quasi-static loads (i.e., loads at frequencies well below the natural frequencies), while the bridle tensions are dominated by the surge and in some cases the pitch natural frequencies. The bridle tensions are not studied any further. The focus of this study is furthermore on the largest platform motions: surge and pitch. The yaw motion is also studied as this motion is expected to be strongly impacted by differences in wind characteristics across turbulence models. The considered motions are illustrated in Figure 4.

The floating wind turbine response subject to the various wind fields is evaluated in terms of DEL of the mooring line and STD of the platform motions. The DEL, R_{eq}, is given by

$$R_{eq} = \left(\frac{\Sigma_i (R_i^m n_i)}{n_{eq}} \right)^{1/m} \tag{8}$$

where R_i is the amplitude of the time series, n_i the number of cycles and n_{eq} the equivalent number of response cycles for an equivalent frequency of 1 Hz in this case. The Wöhler exponent, m, for the mooring line made of chain is assumed to be 3, corresponding to steel. For more information on the procedure for determining DEL, see Nybø et al.[11]

Figure 5 shows the probability distributions of the platform motions and the mooring line tension for the neutral 13 m/s situation. The distributions are all close to Gaussian. A mean surge motion of about 7 m and a mean pitch motion of about 2.7° are observed. The standard deviations of surge and pitch are 0.3–0.9 m and 0.15–0.35° in this case. The mean yaw motion is close to zero with a standard deviation of 0.15–0.3°.

As the focus of this study is to analyse the impact of various wind fields on response, the wind turbine simulations are run without waves and current. In agreement with Mahfouz et al.,[20] the impact of the hydrodynamic forces on the wind turbine structure was found to be small in comparison to the aerodynamic forces. Mahfouz et al. explain this by low hydrodynamic forces on their chosen location, a large wind turbine and large inertia of the physical system. Waves may still cause local forces and fatigue of some components in extreme conditions. Non-linear wave excitation loads and coupled wind-wave effects may excite loads at lower frequencies than the primary wave frequencies. These non-linear load effects are assumed small compared to the direct wind loads on the turbine and are not considered in this work.

In order to analyse the origin of the differences in computed STD and DEL obtained by the different wind formulations, the response spectra are studied. In the response spectra shown, the frequency range is limited to 0–0.05 Hz. As mentioned in Section 1, the natural frequencies of surge, pitch and heave have major impact on the response of a floating wind turbine. These frequencies are all well within the 0- to 0.05-Hz range. The quasi-static response is also expected to be highest in this range, considering the large amplitudes of the wind loading at low frequencies

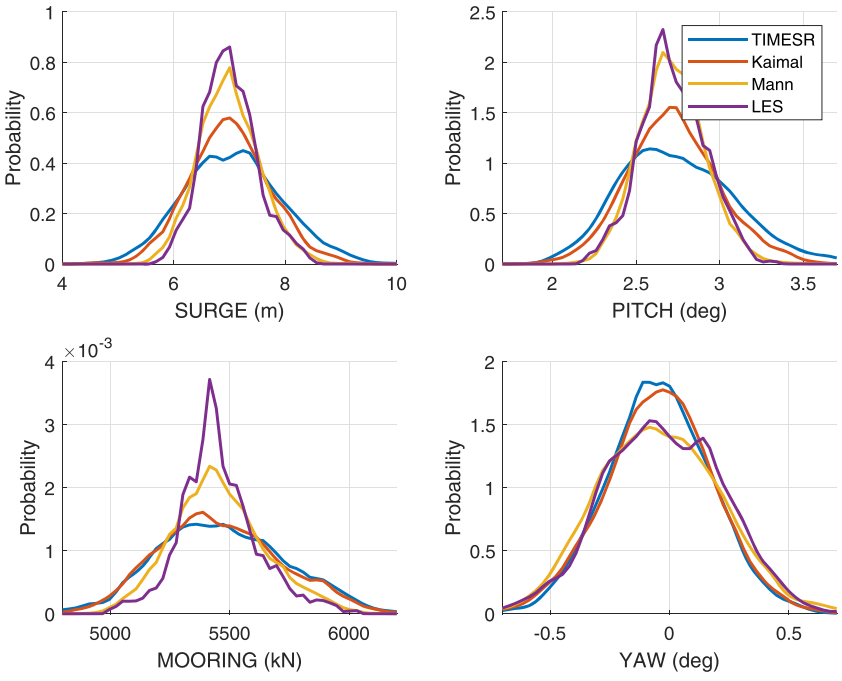

FIGURE 5 Response distribution of platform motions and mooring line tension in the neutral 13 m/s situation

(Figure 1). Higher frequencies than 0.05 Hz are therefore considered to have minor impact on the damage and motions of the specific floating wind turbine of this study.

3 | RESULTS AND DISCUSSION

In the following, the differences in the floating wind turbine response from using TIMESR, Kaimal, Mann or LES input wind fields are analysed in detail. First, the effect of wind shear, turbulence and especially variations of coherence on the response is studied. Findings of this wind characteristics test are taken into consideration when comparing the response of using TIMESR, Kaimal, Mann or LES.

3.1 | Wind characteristics test

Figures 6 and 7 show the impact of various wind characteristics on response, using the wind fields under 'Wind characteristics test' in Table 2. They also clearly show which frequencies are important for the various motions and the mooring line tension considered in this study. As expected, the natural frequencies of surge and pitch are dominant for the platform surge and pitch motions, respectively. Additionally, the quasi-static load has some impact on the platform surge and pitch motions. Typically for a spar platform, the natural frequency of pitch is also important for the surge motion. The surge-pitch coupling is explained by the vertical position of the point of reference for surge being at the mean sea level, not at the centre of rotation of the platform. The centre of rotation, defined as the vertical position with minimum horizontal displacement, is typically far below the sea level for a spar platform. The location depends upon the external loading and is in most cases close to the centre of gravity. For the structure analysed in the present study, the centre of rotation is approximately 82 m below sea level. The computed mooring line tension shows no peak at the pitch natural frequency but is totally dominated by the surge natural frequency. This is explained by the fact that the mooring lines are attached to the hull at 90 m below sea level, that is, close to the centre of rotation. In contrast to the three responses mentioned, the natural frequencies matter less for platform yaw response, which is dominated by quasi-static response.

In the spectra of the platform surge and pitch motions (top plots of Figures 6 and 7), peaks are observed at a lower frequency than expected from the pitch decay test. The pitch decay test is performed by giving the structure an initial pitch displacement of 10° and releasing it without any external forces acting. Similar decay tests were performed while the wind turbine was operating. Uniform wind fields of a few constant wind speeds were used. The results are illustrated in Figure 8. An increased period of oscillation is observed when the turbine is acting, in particular

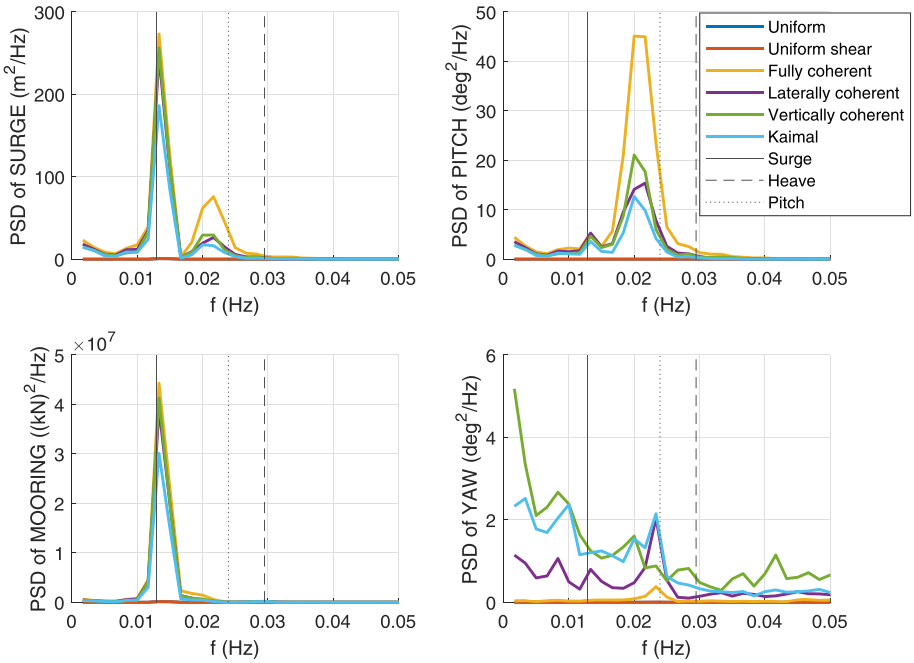

FIGURE 6 Response spectra showing the impact of wind shear, turbulence and positive coherence on platform motions and mooring line tension. The red lines (Uniform shear) lie on top of the dark blue (Uniform). The vertical lines denoted surge, heave and pitch show the corresponding natural frequencies for these modes from OpenFAST decay tests. PSD = power spectral densities

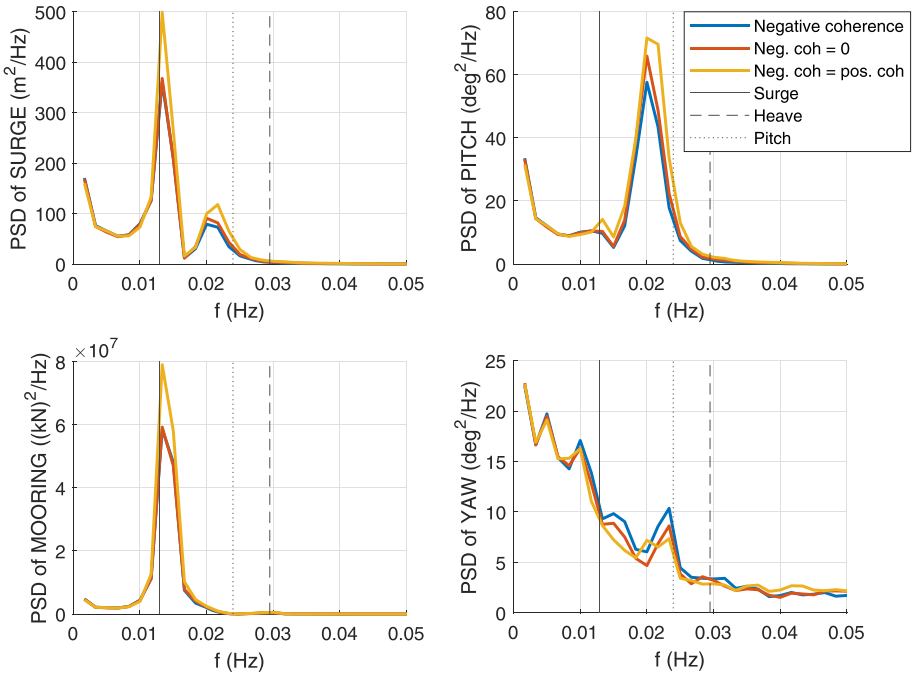

FIGURE 7 Response spectra showing the impact of negative coherence on platform motions and mooring line tension. The red lines lie on top of the blue for surge and mooring. The vertical lines denoted surge, heave and pitch show the corresponding natural frequencies for these modes from OpenFAST decay tests. PSD = power spectral densities

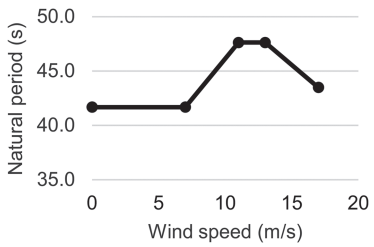

FIGURE 8 Pitch decay periods with various incident wind speeds

close to the rated wind speed. To investigate this phenomenon further, OpenFAST simulations with uniform wind fields of harmonic oscillatory wind speeds were performed. Mean wind speeds of 7 and 13 m/s were used. The wind speed was varied harmonically with an amplitude of 1 m/s. The period of oscillation was varied between 40 and 50 s in steps of 0.5 s. For 7 m/s mean wind speed, maximum pitch response was obtained for a period of oscillation of 40.5 s, while for 13 m/s, the period of maximum pitch response was 48 s, confirming the trends of Figure 8. Our results are in accordance with Souza and Bachynski,[36] who explain the increased pitch natural period by an apparent inertia and damping effects induced by the thrust force on the wind turbine. The sensitivity of pitch natural period to wind speed proves the importance of performing coupled analysis in the design of wind turbines. In the spectra of the platform yaw motion (bottom right plots of Figures 6 and 7), a peak is observed at the roll natural frequency. The roll natural frequency is almost identical to the pitch natural frequency obtained at zero wind speed. The observed yaw motion at this frequency is thus due to a roll–yaw coupling.

Comparing steady, uniform wind fields with and without shear, it is found that the wind shear has negligible impact on the surge and pitch motions and the mooring line tension. However, adding the wind shear approximately doubles the STD of the yaw motion. This is due to increased roll motion at the natural frequency. As the responses are small, this effect is not visible in Figure 6. The combination of blade rotation and wind shear force in the rotor plane causes higher STD of roll. Consequently, the centre of the rotor plane deviates from the tower axis, causing higher STD of yaw. The extreme increase of yaw STD described above is observed only with no turbulence present. The effect of wind shear in a turbulent wind field was investigated further by comparing the response of using a Mann input wind field with a power law coefficient of 0.06 and 0. The differences in roll and yaw STD were less than 1%. Consequently, no impact of the minor differences in wind shear in the turbulent wind fields Kaimal, Mann, TIMESR and LES is expected on response.

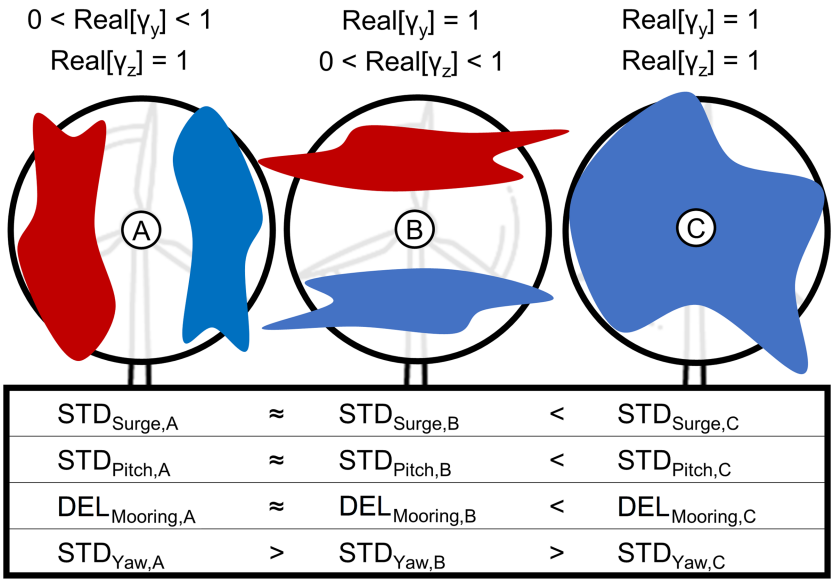

FIGURE 9 Illustration of the impact of coherence on platform motions STD and mooring line DEL. Different colours represent uncorrelated eddies. Case A illustrates a case where there is large coherence in the vertical direction over a length scale similar to the rotor diameter; that is, the dynamic wind speed is similar over this length scale. In the horizontal direction, the coherence is assumed to be lower, causing uncorrelated variations in the wind speed between the two sides of the rotor disc. In case B, large coherence in the horizontal direction is assumed, while there are uncorrelated variations in the wind speed in the vertical direction. In case C, the flow is assumed coherent over most of the rotor disc. As indicated in the table, the three cases excite the different modes of motion differently

Figure 6 shows that higher turbulence levels cause higher energy levels in the complete frequency range, as was found for a bottom-fixed wind turbine in Nybø et al.[11] Without any turbulence (Uniform and Uniform shear), any significant response is only seen at the natural frequencies of the system. Based on this, the variations in turbulence levels between TIMESR, Kaimal, Mann and LES (see, e.g., TI intervals in Table 1) are expected to influence response.

A completely coherent wind field (Fully coherent) causes higher surge and pitch motions and corresponding mooring line tension compared to a more realistic wind field like Kaimal (keep in mind that Kaimal refers to the Kaimal wind spectrum and IEC exponential coherence model). This is especially clear for the motions at the pitch natural frequency, dominant for the pitch motion. A fully coherent wind field causes increased total loads on the rotor and correspondingly large pitch motions. The platform pitch STD is 84% higher when using the fully coherent wind field in comparison to Kaimal, while the surge STD is 38% higher and the mooring DEL 27% higher. The same trends were seen for the tower base of the bottom-fixed wind turbine in Nybø et al.[11] The surge and pitch motions and the mooring line tension are independent of the direction of coherence. The global pitch motion is dominated by the thrust force times the distance between the rotor centre and the water line rather than the local force distribution over the rotor disc. Considering local response, such as the tower top damage equivalent bending moment, the vertical distribution of forces over the rotor disc is the key driver. Thus, the vertical coherence is an important parameter. This expectation is confirmed for a bottom-fixed wind turbine in Nybø et al.[11] The dynamic yaw motion increases significantly with less coherence, especially less horizontal coherence. As seen in Nybø et al.,[11] a wind field with low coherence and corresponding large local forces over the rotor causes high local moments. Specifically, we see the same behaviour in the yaw motions of the floater and the tower yaw moment of the bottom-fixed wind turbine. The impact of coherence on response described above is illustrated in a simplified manner in Figure 9.

When using a wind field containing negative coherence in some frequency range, the surge and pitch motions and the mooring line tension are lower in comparison to using a wind field where this negative coherence is replaced by 0 or its positive equivalent; see Figure 7. For frequencies higher than about 0.03 Hz, the same trend is seen for the platform yaw motion, but at lower frequencies, negative coherence causes higher energy levels. Again, the same trends are seen for the tower yaw moment of Nybø et al.,[11] and the yaw motions of the floater considered in the present study.

3.2 | Impact of turbulence model on floater response

In the following, the differences in floater response by using TIMESR, Kaimal, Mann and LES are evaluated. Figure 10 summarizes these differences in terms of STD of the surge, pitch and yaw motions and DEL of the mooring line tension. As expected, the surge and pitch STD and

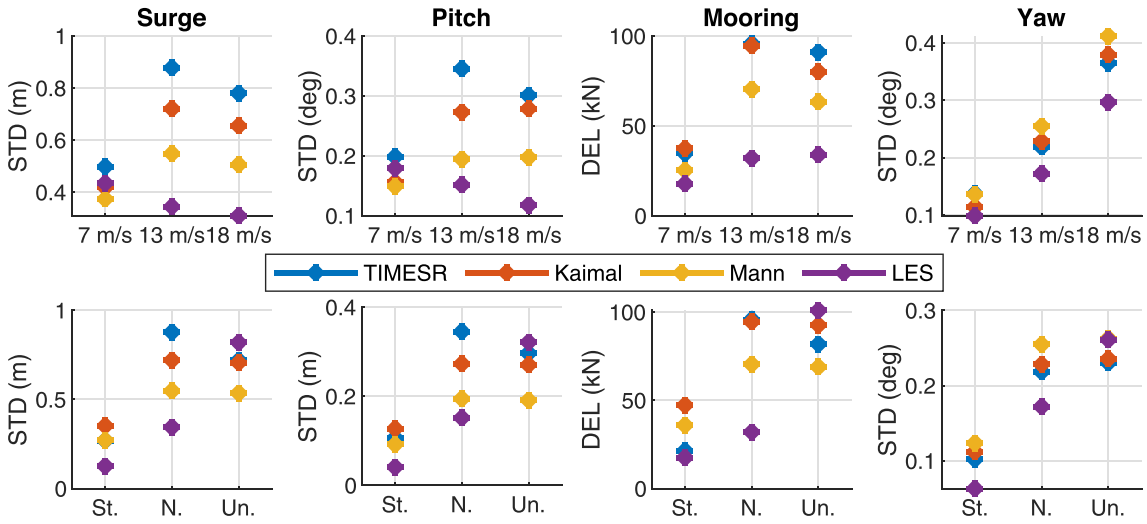

FIGURE 10 Standard deviations (STD) and damage equivalent loads (DEL) of response time series for three wind speeds (top plots) and three atmospheric stability conditions (bottom plots). N. = neutral, Un. = unstable, St. = stable. Mann unstable yaw is at the same value as LES

Response		7 m/s	13 m/s			18 m/s	*Cause*	
Method	**STD/DEL**	**Neutral**	**Stable**	**Neutral**	**Unstable**	**Neutral**	**γ**	**PSD_{Wind}**
Surge (STD), pitch (STD) & mooring line tension (DEL)								
TIMESR	High	■		■		■	High	High
Kaimal	High	■	■	■	■	■	High	
Mann	Low	■	■	■	■	■	Low (-)	
LES	High				■		High	High
LES	Low		■	■		■	Low	Low
Yaw (STD)								
Mann	High	■	■	■	■	■	Low (-)	
LES	High				■			High
LES	Low	■	■	■		■		Low

FIGURE 11 Summary of response (left) and wind characteristics causing this response (right) of using TIMESR, Kaimal, Mann and LES wind fields. Relevant wind speed and atmospheric stability situations are marked in the middle. For example, the surge STD, pitch STD and mooring line DEL of TIMESR are high for all wind speeds in neutral stability conditions due to high coherence and high energy levels of the wind spectra. γ = coherence, (−) = negative, PSD = power spectral densities

mooring line DEL are largest close to the rated wind speed for most wind fields. The STD of the yaw motion, on the other hand, increases with wind speed. Also as expected, stable atmospheric conditions, with corresponding low TI, lead to lower STD and DEL. The trends across turbulence models are similar for the surge and pitch motions and the mooring line tension. When using, for example, the Mann wind field, these are relatively low, while the STD of the yaw motion is rather high. Based on the findings of the wind characteristics test, this indicates that coherence plays an important role. Figure 10 furthermore shows that the response of using the LES wind fields is low in most situations. This may rather be a consequence of a lower turbulence level. The origin of the differences in floater response by using TIMESR, Kaimal, Mann and LES is discussed further in the following. These results are summarized in Figure 11.

Taking a closer look at the surge motions, TIMESR leads to the highest STD for all wind speeds in neutral atmospheric conditions. A similar trend is seen in the stable situation, while the LES wind field leads to highest STD in the unstable situation. These trends are reflected in the response spectra of Figure 12. At the natural frequency of surge, having major impact on the motions, Kaimal and TIMESR cause relatively high energy levels for all situations. The high PSD of using these two in comparison to Mann and LES is expected to be related to the differences in coherence between the wind fields. As observed in Section 3.1, high coherence is expected to cause high surge response at the surge natural

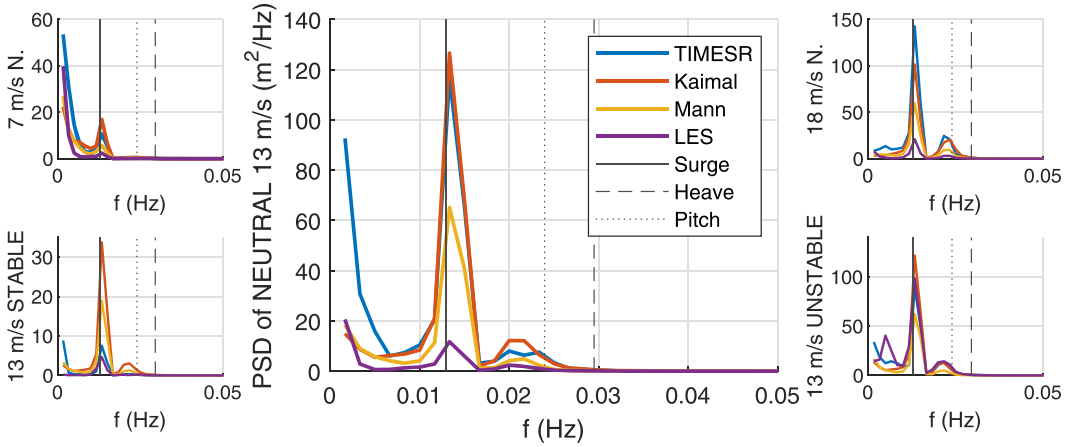

FIGURE 12 Platform surge motions of the floating wind turbine. Top plots, from left to right: 7, 13 and 18 m/s, all neutral stability conditions. Bottom plots, from left to right: stable, neutral and unstable stability conditions, all 13 m/s. The vertical lines denoted surge, heave and pitch show the corresponding natural frequencies for these modes from OpenFAST decay tests. PSD = power spectral densities, N. = neutral

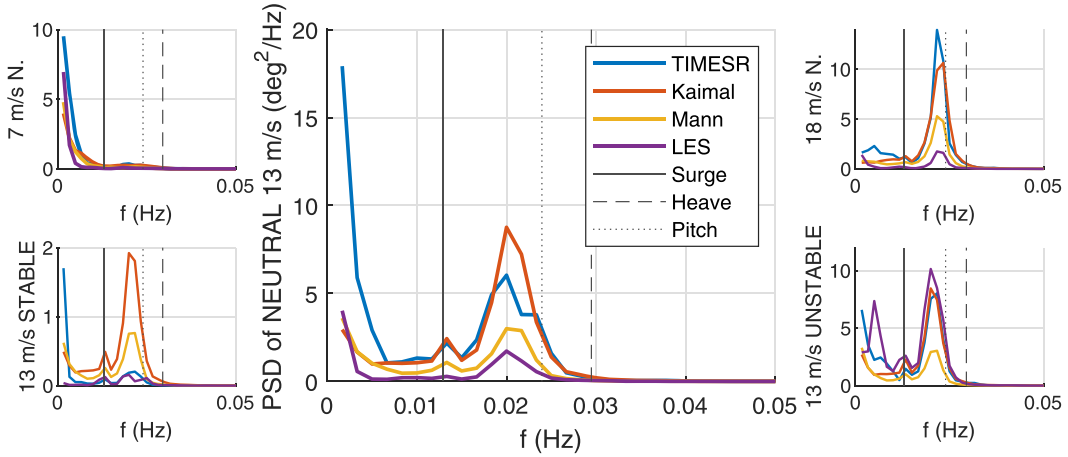

FIGURE 13 Platform pitch motions of the floating wind turbine. Top plots, from left to right: 7, 13 and 18 m/s, all neutral stability conditions. Bottom plots, from left to right: stable, neutral and unstable stability conditions, all 13 m/s. The vertical lines denoted surge, heave and pitch show the corresponding natural frequencies for these modes from OpenFAST decay tests. PSD = power spectral densities, N. = neutral

frequency. Figures 2 and 3 show that the coherence of TIMESR and Kaimal are high in most situations, while the coherence of Mann is low. The differences between Kaimal and Mann in the present study are consistent with the findings of Eliassen and Bachynski.[14,15] They also explain the high surge response of using Kaimal by the more uniform forcing over the rotor. The low coherence of TIMESR in the stable situation is also reflected by a lower response at the surge natural frequency.

The quasi-static response impacts the surge STD as well, especially for the low wind speed (top left plot of Figure 12). At these low frequencies, there are clear similarities between the response spectra and the wind spectra, where the TIMESR wind fields generally have high energy levels. These high energy levels correspond to large variations in the mean wind speed or non-stationary conditions. The stationary turbulence models defined by the IEC standard, Mann and Kaimal, are not able to reproduce these large scale fluctuations. They are originally intended for small onshore wind turbines with high natural frequencies in comparison to floating wind turbines. In the design of onshore wind turbines, shorter time series are thus required in order to evaluate the dynamic response. Typically, 10-min time series are used for onshore wind turbine design, while 1-h or even longer time series are required for floating wind turbine design. The longer the time series, the more large scale fluctuations are seen in observations. The high energy levels at very low frequencies in the TIMESR wind fields, and corresponding high energy levels in the surge motion at similar frequencies, show that large scale fluctuations should be modelled in input wind fields. This is as mentioned not possible by the turbulence models defined by the IEC standard. Available options for representing large scale fluctuations are, for example, the TIMESR model used in the present study, adding large scale fluctuations to the standard Kaimal and Mann models, or LES with configurations allowing for large

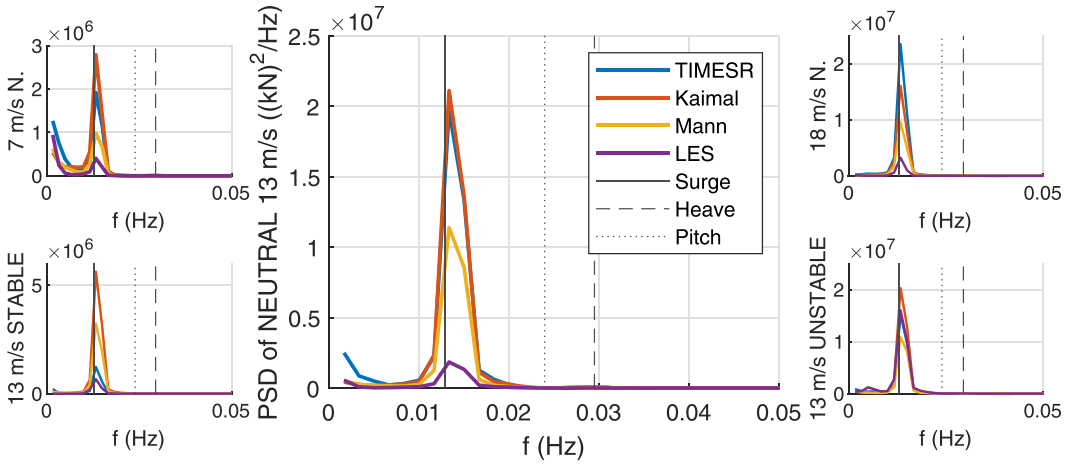

FIGURE 14 Mooring line tension of the floating wind turbine. Top plots, from left to right: 7, 13 and 18 m/s, all neutral stability conditions. Bottom plots, from left to right: stable, neutral and unstable stability conditions, all 13 m/s. The vertical lines denoted surge, heave and pitch show the corresponding natural frequencies for these modes from OpenFAST decay tests. PSD = power spectral densities, N. = neutral

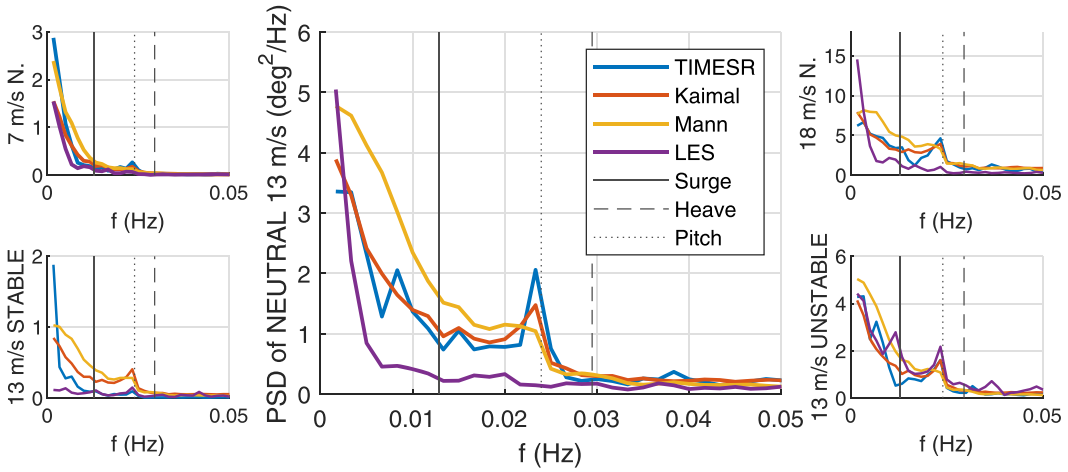

FIGURE 15 Platform yaw motions of the floating wind turbine. Top plots, from left to right: 7, 13 and 18 m/s, all neutral stability conditions. Bottom plots, from left to right: stable, neutral and unstable stability conditions, all 13 m/s. The vertical lines denoted surge, heave and pitch show the corresponding natural frequencies for these modes from OpenFAST decay tests. PSD = power spectral densities, N. = neutral

scale fluctuations. As shown by Nybø et al.,[37] the input parameters of the Mann model may also be fitted to observations in order to approach the high energy levels of the TIMESR wind spectra and corresponding response.

The LES wind fields have high coherence and high energy levels in the unstable situation, which is also reflected by a higher surge STD in Figure 10. In most other situations, the coherence and particularly TI of the LES wind fields are very low, which cause low energy levels for all frequencies.

Figure 10 shows that the same trends are seen for the pitch and surge motions. The STD of TIMESR and Kaimal is in most cases high, while the STD of Mann and LES is lower. Kaimal is found to cause higher pitch STD than Mann for the different platforms analysed by Eliassen and Bachynski[14,15] as well. Together with the quasi-static frequency region, the natural frequency of pitch is dominant for the pitch motion (Figure 13). The trends of pitch PSD at pitch natural frequency are similar to the surge PSD at the surge natural frequency. At 7 m/s, there is relatively low energy levels at the pitch natural frequency due to a large positive thrust gradient which damps the system. The response spectra at this wind speed are therefore a reflection of the wind spectra, with, for example, a similar trend of Mann and Kaimal.

The differences in coherence between TIMESR, Kaimal, Mann and LES cause the differences in the mooring line DEL. Kaimal and TIMESR, which have the highest coherence in most situations, cause the highest DEL. In Doubrawa et al.[17] they rather found that the mooring line DEL was larger when using Mann instead of Kaimal. In Eliassen and Bachynski,[14,15] the order of Mann and Kaimal was found to be dependent on wind

speed. The mooring line tensions and the corresponding order of Mann and Kaimal depend on the floater and mooring design. Figure 14 shows that, for the design used in the present study, the surge motions are dominant for all wind speeds. The high DEL of using Kaimal, as seen in the surge STD, is therefore according to expectations. Relative to the pitch and surge motions, the differences in turbulence level of the wind fields have less impact on the differences in mooring line tensions. Figure 10 shows that the TIMESR DEL is correspondingly lower.

In contrast to the surge and pitch motions and the mooring line tension, the Mann wind fields cause large yaw STD. This is reflected in the response spectra of Figure 15, especially at frequencies lower than the pitch natural frequency. Based on the findings of Section 3.1 and Figure 3, it is clear that the low and negative horizontal coherence of Mann cause these high energy levels. Godvik,[16] Putri et al,[12] and Eliassen and Bachynski[14,15] also observed a large STD of Mann compared to Kaimal in the yaw motion. Some of the LES wind fields have low horizontal coherence as well. However, their low turbulence levels dominate the PSD of yaw motions.

The trends across turbulence models are similar in the yaw STD of the floater and the damage equivalent moment of the tower top yaw in Nybø et al.[11] The Mann wind fields cause high yaw response in all situations considered. The same similarities are found between the other considered responses of the floater (platform surge STD, platform pitch STD and mooring line DEL) and the tower bottom fore-aft bending moment of the bottom-fixed wind turbine. In most of the situations, TIMESR and Kaimal cause the highest motions and damage relative to Mann. The LES wind fields cause low overall STD and DEL due to the low turbulence levels.

4 | CONCLUSIONS

This study challenges the applicability of the standard turbulence models, Kaimal and Mann, by studying the wind induced response of a large floating wind turbine subject to Kaimal, Mann, LES and TIMESR wind fields. More specifically, the surge, pitch and yaw motions of the floater and corresponding fatigue damage of a mooring line are analysed. For the 15-MW floating wind turbine with spar foundation analysed in this study, the surge motions are dominant for the mooring line tension.

First, the impact of various wind characteristics on the dynamic response of the floating wind turbine is evaluated. Wind shear is found to have negligible impact on the platform motions and the mooring line tension considered. As expected, turbulence greatly impacts all considered platform motions and the mooring line tension over the entire frequency range. A coherent wind field causes higher surge and pitch STD and mooring line DEL in comparison to a wind field with less coherence over separation distances in the order of the rotor diameter. The yaw STD is increased when the horizontal coherence becomes low or even negative over such distances.

The differences in floater response of using Mann versus Kaimal wind fields are significant. The turbulence intensities, mean wind speeds, wind shear and wind spectra are equivalent in the two models. It is rather the differences in coherence between the two that cause the differences in response. Kaimal, with higher coherence, causes larger surge and pitch STD, and corresponding larger mooring line DEL. Mann, with lower and even negative horizontal coherence, causes higher STD of the yaw motion. The differences in platform surge, pitch and yaw STD of using the Kaimal or Mann wind fields are consistent with previous findings.

In contrast to Mann and Kaimal, TIMESR and LES take atmospheric stability into account in the generation of turbulent structures. In the unstable situation, large and energetic coherent structures are present in these wind fields, causing corresponding high STD of the surge and pitch motions in comparison to the standard models. In the stable situation, on the other hand, smaller and less energetic eddies present in TIMESR and LES cause low motion and mooring line response.

Great similarities are found in the response analysis of the floater structure of the present study and the bottom-fixed wind turbine of Nybø et al.[11] The same trends across turbulence models are seen in the surge and pitch motions and the mooring line tension as in the tower bottom fore-aft bending moment. Similarly, the yaw motion and tower yaw bending moment react equivalently to differences in coherence. However, the differences across turbulence models are larger for the floater, having natural frequencies in the frequency range where large variations in the wind fields exist.

Using LES wind fields, generally low motion and mooring line responses are observed relative to the standard models. This is attributed to the low TI achieved and, in particular, the low energy levels in the low frequency range of the LES wind spectra. It is challenging to tune LES outputs to observations with limited information on the atmospheric conditions, especially in the neutral situations. LES may create far more realistic wind fields than simple models such as Kaimal and Mann but may still cause less realistic response if failing to reproduce important wind characteristics such as TI. The great impact of TI on response shows the importance of measuring turbulence at site and accurately represent TI in the design process of offshore wind turbines.

TIMESR, using measured wind velocities as input, causes larger motion and mooring line responses than the standard turbulence models in most of the situations considered. This is partly due to the presence of large scale, low-frequency fluctuations captured by TIMESR. Such low-frequency phenomena are not modelled in the stationary (standard) turbulence models: Kaimal and Mann. This study clearly demonstrates that both standard turbulence models are consequently likely to underestimate the surge and pitch response of the floating wind turbine. The higher coherence estimates obtained by the TIMESR model also lead to higher surge and pitch STD and corresponding higher mooring line DEL. The TIMESR yaw STD is low compared to the yaw predicted using the standard turbulence models. This is a combined effect of the frequency

distribution of turbulence and the horizontal coherence. Due to lack of measurements, little is known about the horizontal coherence. This study demonstrates the need for improved knowledge about the coherence of the wind field. This need increases with the diameter of the rotor.

ACKNOWLEDGEMENTS

The authors would like to thank Vegard Milde, an MSc student at the University of Bergen, for cooperation on the OpenFAST model of the spar floater. For providing LES wind fields and associated support, we would like to thank Matthew J. Churchfield at the National Renewable Energy Laboratory. A portion of the research was performed using computational resources sponsored by the Department of Energy's Office of Energy Efficiency and Renewable Energy and located at the National Renewable Energy Laboratory.

PEER REVIEW

The peer review history for this article is available at https://publons.com/publon/10.1002/we.2712.

DATA AVAILABILITY STATEMENT

The data that support the findings of this study are available from the corresponding author upon reasonable request.

ORCID

Astrid Nybø https://orcid.org/0000-0002-7438-7936

REFERENCES

1. International Renewable Energy Agency. Future of wind: deployment, investment, technology, grid integration and socio-economic aspects (A Global Energy Transformation paper). tech. rep., Abu Dhabi, IRENA; 2019. https://www.irena.org/-/media/Files/IRENA/Agency/Publication/2019/Oct/IRENA_Future_of_wind_2019.pdf. Accessed July 2, 2021.
2. International Energy Agency. Offshore wind outlook 2019, Paris, IEA; 2019. https://iea.blob.core.windows.net/assets/495ab264-4ddf-4b68-b9c0-514295ff40a7/Offshore_Wind_Outlook_2019.pdf. Accessed July 2, 2021.
3. Wind Europe. Our energy, our future. tech. rep., Brussels, Wind Europe; 2019. https://windeurope.org/wp-content/uploads/files/about-wind/reports/WindEurope-Our-Energy-Our-Future.pdf. Accessed July 2, 2021.
4. International Electrotechnical Commision. IEC 61400-1 Wind energy generation systems - Part 1: design requirements. tech. rep., Geneva, IEC; 2019. https://webstore.iec.ch/publication/26423. Accessed July 2, 2021.
5. International Electrotechnical Commision. IEC 61400-3-1:2019 Wind energy generation systems - Part 3-1: design requirements for fixed offshore wind turbines. tech. rep., Geneva, IEC; 2019. https://webstore.iec.ch/publication/29360. Accessed July 2, 2021.
6. International Electrotechnical Commision. IEC TS 61400-3-2:2019 Wind energy generation systems - Part 3-2: design requirements for floating offshore wind turbines. tech. rep., Geneva, IEC; 2019. https://webstore.iec.ch/publication/29244. Accessed July 2, 2021.
7. Kaimal JC, Wyngaard JC, Izumi Y, Coté OR. Spectral characteristics of surface-layer turbulence. *Q J Roy Meteor Soc*. 1972;98(417):563-589.
8. Mann J. The spatial structure of neutral atmospheric surface-layer turbulence. *J Fluid Mech*. 1994;273:141-168.
9. Jonkman BJ. TurbSim User's Guide v2.00.00. tech. rep., Golden, NREL; 2016.
10. Nybø A, Nielsen FG, Reuder J, Churchfield M, Godvik M. Evaluation of different wind fields for the investigation of the dynamic response of offshore wind turbines. *Wind Energy*. 2020;23(9):1810-1830.
11. Nybø A, Nielsen FG, Godvik M. Quasi-static response of a bottom-fixed wind turbine subject to various incident wind fields. *Wind Energ*. 2021:1-19.
12. Putri RM, Obhrai C, Jakobsen JB, Ong MC. Numerical analysis of the effect of offshore turbulent wind inflow on the response of a spar wind turbine. *Energies*. 2020;13(10):1-22. https://doi.org/10.3390/en13102506
13. Putri RM, Obhrai C, Jakobsen JB. Response sensitivity of a semisubmersible floating offshore wind turbine to different wind spectral models. *J Phys Conf Ser*. 2020;1618:22012.
14. Eliassen L, Bachynski EE. The effect of turbulence model on the response of a large floating wind turbine. In: ASME 2017 36th Int Conf Ocean, Offshore and Arctic Engineering. Trondheim, Norway; 2017. https://doi.org/10.1115/OMAE2017-61179
15. Bachynski EE, Eliassen L. The effects of coherent structures on the global response of floating offshore wind turbines. *Wind Energy*. 2019;22(2):219-238.
16. Godvik M. Influence of wind coherence on the response of a floating wind turbine. *Science meets Industry*. Stavanger, Norway; 2016. http://www.norcowe.no/doc//konferanser/2016/SMIStavangerpresentasjoner/GodvikStatoilInfluenceofthewindcoherenceontheresponseofafloatingwindturbine.pdf
17. Doubrawa P, Churchfield MJ, Godvik M, Sirnivas S. Load response of a floating wind turbine to turbulent atmospheric flow. *Appl Energ*. 2019;242:1588-1599. https://doi.org/10.1016/j.apenergy.2019.01.165
18. Myrtvedt MH, Nybø A, Nielsen FG. The dynamic response of offshore wind turbines and their sensitivity to wind field models. *J Phys Conf Ser*. 2020;1669:12013.
19. Gaertner E, Rinker J, Sethuraman L, et al. Definition of the IEA 15-Megawatt offshore reference wind turbine. Tech. Rep. NREL/TP-5000-75698, Golden, NREL; 2020. https://www.nrel.gov/docs/fy20osti/75698.pdf. Accessed July 2, 2021.
20. Mahfouz MY, Salari M, Hernández S, et al. Public design and FAST models of the two 15MW floater-turbine concepts. tech. rep., Stuttgart, University of Stuttgart; 2020. http://corewind.eu/wp-content/uploads/files/publications/COREWIND-public-design-and-FAST-models-of-the-two-15mw-floater-turbine-concepts.pdf. Accessed July 2, 2021.
21. Obukhov AM. Turbulence in an atmosphere with a non-uniform temperature. *Bound.-Layer Meteorol*. 1971;2(1):7-29.

22. Van Wijk AJM, Beljaars ACM, Holtslag AAM, Turkenburg WC. Evaluation of stability corrections in wind speed profiles over the North Sea. *J Wind Eng Indust Aerodyn*. 1990;33(3):551-566.
23. Danmarks Tekniske Universitet. Mann 64bit turbulence generator. https://www.hawc2.dk/download/pre-processing-tools. Accessed July 2, 2021; 2018.
24. Churchfield M, Lee S, Moriarty P. Overview of the Simulator fOr Wind Farm Application (SOWFA). tech. rep., Golden, NREL; 2012. https://www.nrel.gov/wind/nwtc/assets/pdfs/sowfa-tutorial.pdf. Accessed July 2, 2021.
25. FuE-Zentrum FH Kiel GmbH. FINO1: Forschungsplattformen in Nord- und Ostsee Nr. 1. http://www.fino1.de/en/. Accessed July 2, 2021; 2019.
26. Nybø A, Nielsen FG, Reuder J. Processing of sonic anemometer measurements for offshore wind turbine applications. *J Phys Conf Ser*. 2019;1356:12006.
27. Cheynet E, Jakobsen JB, Reuder J. Velocity spectra and coherence estimates in the marine atmospheric boundary layer. *Bound Layer Meteorol*. 2018;169(3):429-460.
28. National Renewable Energy Laboratory. GitHub - OpenFAST. https://github.com/openfast. Accessed July 2, 2021; 2021.
29. Cheynet E, Jakobsen JB, Snæbjörnsson J, et al. Application of short-range dual-Doppler lidars to evaluate the coherence of turbulence. *Exp Fluids*. 2016;57:1-17.
30. Welch PD. The use of fast Fourier transform for the estimation of power spectra: a method based on time averaging over short, modified periodograms. *IEEE Trans Audio Electroacoust*. 1967;15(2):70-73.
31. Vázquez D'andrea JM. Study of the motions and nacelle accelerations of the Windcrete floating offshore wind turbine according to the IEC 64100-3 procedure. *Master's Thesis*: Escola Tècnica Superior d'Enginyeria Industrial de Barcelona. Barcelona; 2020.
32. National Renewable Energy Laboratory. GitHub - NREL/ROSCO. https://github.com/NREL/ROSCO. Accessed July 2, 2021; 2021.
33. Ziegler JG, Nichols NB. Optimum settings for automatic controllers. *Trans ASME*. 1942;64(11):759-765.
34. Skaare B, Hanson TD, Nielsen FG. Importance of control strategies on fatigue life of floating wind turbines. In: Proc Int Conf OMAE. San Diego, California, USA; 2007:493-500. https://doi.org/10.1115/OMAE2007-29277
35. Skaare B. Development of the hywind concept. In: Proc Int Conf OMAE. Trondheim, Norway; 2017. https://doi.org/10.1115/OMAE2017-62710
36. Souza CES, Bachynski EE. Changes in surge and pitch decay periods of floating wind turbines for varying wind speed. *Ocean Eng*. 2019;180:223-237.
37. Nybø A, Nielsen FG, Godvik M. Analysis of turbulence models fitted to site, and their impact on the response of a bottom-fixed wind turbine. *J Phys Conf Ser*. 2021;2018:12028.

How to cite this article: Nybø A, Gunnar Nielsen F, Godvik M. Sensitivity of the dynamic response of a multimegawatt floating wind turbine to the choice of turbulence model. *Wind Energy*. 2022;25(6):1013-1029. doi:10.1002/we.2712